DOI: 10.1002/chem.200800129

Morphology-Controlled Assembly of ZnO Nanostructures: A Bioinspired Method and Visible Luminescence

Gousia Begum,[a] Sunkara V. Manorama,[a] Shashi Singh,[b] and Rohit Kumar Rana*[a]

Abstract: In a bioinspired methodology, positively charged polypeptides and polyamines directly catalyse ZnO mineralization under "green" conditions of room temperature and neutral pH. The polyamines not only act as mineralizing agents for the formation of ZnO nanoparticles, but also self-assemble the nanoparticles to form spindle-like morphologies at these very ambient conditions. Both the directional growth of ZnO and its luminescent property have a pH dependency. At higher pH, the ZnO shape changes to a rodlike morphology that exhibits green photoluminescence with different intensity than that for ZnO spindles.

Keywords: biomimetic synthesis · luminescence · nanomaterials · polyamines · self-assembly

Introduction

Biomineralization is the process by which nature produces biominerals with exquisite nanostructures under inherently benign conditions of low temperature, ambient pressure and near-neutral pH. It is of immense interest for materials scientists to learn how to create and control such nanostructures that resemble the naturally existing biominerals. The recent discovery of silaffin peptides, long-chain polyamines[1] and the silicatein[2] molecules responsible for biomineralization has resulted in initial headway in understanding the processes. The biospecific interaction of these molecules with inorganic materials has been the key to potential assembly capabilities for generating new organized materials. This bioinspired morphosynthesis has lately been emerging as an important environmentally friendly "green" route to generate inorganic materials with controlled morphologies by using bioextracts or related molecules as structure-directing agents.[3] Herein, we report an extremely facile bioinspired method to synthesize ZnO nanostructures at room temperature and neutral pH conditions by using polypeptides and polyamines as the additives.

ZnO, a versatile semiconductor with a wide, direct band gap of 3.37 eV, has diversified industrial applications in the fields of electronics, photoelectronics, sensors, catalysis and photocatalysis.[4] The strong dependency of its property on the structure and morphology, which includes the recent demonstration of ultraviolet lasing from nanowires,[5] has stimulated the search for new synthetic methodologies for well-controlled ZnO nanostructures with interesting morphologies.[6] Several reports on high-temperature physical or chemical methods for syntheses have been published.[7] However, wet-chemical approaches carried out under mild conditions are attracting a growing interest. A few methods for preparing ZnO at low temperatures have been reported, but usually requiring strong alkali media.[8] Oliveira et al. obtained an ellipsoidal morphology using $Zn(NO_3)_2$ and NaOH solution at room temperature under double-jet conditions at pH 9.5.[9] Kisailus et al. developed a low-temperature vapour-diffusion-based method in which ammonia vapour diffuses through the surface of a solution of a molecular precursor to slowly catalyse the formation of zinc oxide and vectorially regulate the growth of nanostructured thin films.[10a] Zhang et al. reported the near-room-temperature production of highly oriented and densely packed ZnO nanoarrays by natural oxidation of zinc metal in a mixture of formamide and water.[10b]

Proteins or biomolecules are rarely employed for mineralization of ZnO because of their complexity and the demand of extremely mild experimental conditions necessary to pre-

[a] G. Begum, Dr. S. V. Manorama, Dr. R. K. Rana
Nanomaterials Laboratory, Inorganic and
Physical Chemistry Division
Indian Institute of Chemical Technology
Hyderabad-500 007 (India)
Fax: (+91) 40-27160921
E-mail: rkrana@iict.res.in

[b] Dr. S. Singh
Centre for Cellular and Molecular Biology
Hyderabad-500 007 (India)

Supporting information for this article is available on the WWW under http://www.chemeurj.org or from the author.

serve their physical and chemical properties.[11] Instead, many researchers have used synthetic polymers as substitutes to prepare ZnO nanostructures with different shapes, sizes and crystal phases.[12] The polymers are generally selected to have negatively charged moieties that preferably interact with Zn^{2+} ions. The electrostatic interaction induces a directional growth of the formed structure. For example, single-crystalline hexagonal discs and rings of ZnO morphologies resulted when using an anionic surfactant, sodium bis(2-ethylhexyl) sulfosuccinate, to preferentially interact with the Zn^{2+} (0001) surface of ZnO.[13] Bauermann et al. reported the synthesis of ZnO hexagonal plates using gelatin as the organic matrix, in which the suggested mechanism involved an electrostatic interaction between the positively charged Zn^{2+}–water complex and the negatively charged carboxylic groups of the gelatin.[11a] To substantiate such electrostatic interaction, Wegner's group analysed the forces between carboxylic-functionalized latex nanoparticles and differently terminated zinc oxide surfaces by atomic force microscopy.[14] The results convincingly demonstrated a preferred adhesion of the latex particles to zinc-terminated ZnO (0001) faces compared with oxygen-terminated and apolar faces. In a separate experiment as an alternative to the negatively charged molecules, Umetsu et al. found a few peptide sequences with basic (positively charged) and hydrophobic residues to exhibit stronger binding for ZnO.[11b] However, these peptides did not catalyse the ZnO mineralization. The peptide was then modified by conjugating with a glycine linker that had a cysteine residue to catalyse ZnO formation from $Zn(OH)_2$. Herein, we report that positively charged, simple polypeptides and related polyamines can directly catalyse ZnO formation in a wet-chemical method under "green" conditions. Interestingly, the polyamines not only act as mineralizing agents for ZnO nanoparticles, but also self-assemble the nanoparticles to form spindle- and rodlike morphologies under these ambient conditions.

Results and Discussion

Mineralization: Representative TEM images of the as-synthesized samples obtained from the hydroxide precursor using polyamine (poly(allylamine hydrochloride) (PAH), 70 kDa, 2 mg mL^{-1}) and polypeptide (poly(L-lysine hydrobromide) (PLL), 150 kDa, 2 mg mL^{-1}) as mineralizers under mild conditions (RT and pH ≈ 7.3) are shown in Figure 1. Irrespective of the type of polyamine, predominantly spindle-shaped particles were observed. The particles are of similar sizes with 300–500 nm width and 700–1500 nm length. A few particulates of smaller sizes (10–20 nm) were also observed. The XRD patterns of the corresponding as-synthesized samples obtained with PAH and PLL are shown in Figure 1b and d, respectively. In both cases, the XRD peaks are indexed to the typical wurtzite hexagonal phase of ZnO (JCPDS card No. 36–1451) with lattice constants of $a = 3.259$ and $c = 5.196$ Å. The absence of any other peaks, due to either the precursor or any impurities, indicates that phase-pure ZnO is produced under these extremely mild synthesis conditions. The atomic absorption spectroscopic (AAS) analysis of the supernatant showed an 85% yield for ZnO conversion from the hydroxide precursor. The remaining amount of zinc present in the supernatant suggests that ZnO formation may involve solubilization of the solid hydroxide precursor into the solution.

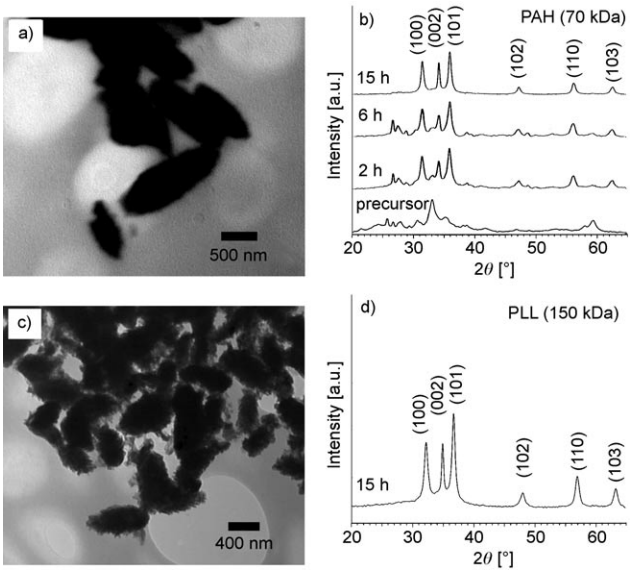

Figure 1. a), c) TEM images of the materials synthesized from the precursor and a) 70 kDa PAH or c) 150 kDa PLL at RT and pH 7.3 or 7.5, respectively, for a reaction duration of 15 h. b), d) The corresponding XRD patterns; b) also includes the XRD patterns of the precursor and the materials obtained with PAH (70 kDa) after 2 and 6 h of reaction.

As seen from the XRD patterns of the samples obtained after various reaction times (Figure 1c and Table 1), the formation of ZnO from the precursor starts at the very beginning (2 h) of the reaction although some amount of precursor still remains. Further increase in the reaction time converted more of the precursor to ZnO. After 15 h of continuous stirring, XRD peaks arising from the precursor disappeared with the emergence of a phase-pure ZnO structure. The hydroxide precursor that had a flake-like morphology converted into aggregates of spindle-like structure after interaction with the polyamines (see Figures S1–S3 in the Supporting Information). The crystallite size of ZnO estimated from XRD by using the Debye–Scherrer formula is 11–16 nm (Table 1). This value compares well with the sizes (10–20 nm) of the smallest particulates seen along with the spindle-shaped particles in the TEM images, thus indicating that the spindle shapes are probably aggregates of many smaller crystallites of nanometre size.

To study the role of polyamines, the reaction was carried out in the absence and presence of different concentrations of these species under similar reaction conditions. Without the presence of polyamine, the precursor remained unchanged even after 2 days of continuous stirring. So, the presence of polyamine is crucial in the mineralization of ZnO. The use of PAH with a lower molecular weight

Table 1. Various mineralizing agents used, synthesis conditions employed, the corresponding products and crystallite sizes of the ZnO obtained.

Mineralizing agent	c [mg mL^{-1}][a]	pH	t [h]	Product[b,c]	Crystallite size [nm][d]
PAH (70 kDa)	2.0	7.3	2	O*+H	11.0
PAH (70 kDa)	2.0	7.3	6	O*+H	11.0
PAH (70 kDa)	2.0	7.3	15	O	15.4
PAH (15 kDa)	2.0	7.1	15	O	11.0
PAH (15 kDa)	2.0	8.6	2	O	12.8
PAH (15 kDa)	2.0	8.6	15	O	12.9
PAH (15 kDa)	0.8	7.4	15	O*+H	12.8
PLL (150 kDa)	2.0	7.5	15	O	12.8
PLL (1–5 kDa)	2.0	7.3	15	O	19.2
PDADMAC	2.0	7.8	15	O	15.4
KOH	0.3	11.2	15	O	15.4
KOH	0.15	10.9	15	O*+H	12.4
KOH	0.01	8.2	15	O+H*	–

[a] Concentration of the mineralizing agent. [b] "O" represents ZnO and "H" represents $Zn(OH)_2$. [c] "*" indicates percentage of the excess species. [d] Crystallite size is determined from XRD peaks using the Scherrer formula. PDADMAC: poly(diallyldimethylammonium chloride).

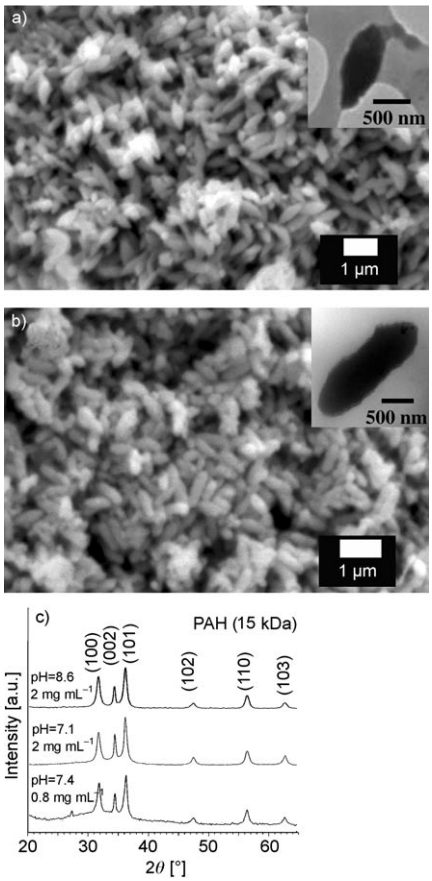

Figure 2. a), b) SEM images of the materials obtained by reacting the precursor with a) PAH (15 kDa, 0.8 mg mL^{-1}) at RT and pH 7.4 (inset: the corresponding TEM image), and b) PAH (15 kDa, 2.0 mg mL^{-1}) at RT and pH 8.6 for a reaction duration of 15 h (inset: the corresponding TEM image). c) XRD patterns of materials synthesized from the precursor and various concentrations of PAH (15 kDa) at RT for 15 h at different pH values.

(15 kDa, 2 mg mL^{-1}) as mineralizing agent under similar conditions also resulted in ZnO formation (see Figure 2c and Figure S4a in the Supporting Information). The morphology of these particles is same as that seen with the higher-molecular-weight PAH (70 kDa). The TEM image also shows the presence of smaller particles of size 10–20 nm in the near vicinity of the spindle-shaped particles (see Figure S4a in the Supporting Information). The formation of ZnO with similar morphologies could also be achieved with a very low concentration of PAH (15 kDa, 0.8 mg mL^{-1}; see Figure 2a and Figure S4b in the Supporting Information), although the product contained a very small amount of unreacted precursor (see Figure 2c). However, at the higher concentration of PAH (2.0 mg mL^{-1}) pure ZnO phase was obtained. We found this polyamine-mediated ZnO mineralization to be broadly applicable, as the use of other polyamines with different molecular weights, such as PLL (1–5 kDa) and PDADMAC (100–200 kDa), also produced ZnO under similar "green" conditions (Table 1).

Effect of pH: The effect of the pH on the formation and morphology of ZnO was studied. The pH of the solution was increased by adding an alkali solution (see Table 1). As revealed by AAS analysis of the supernatant, with an increase in the pH to 8.6 the product yield increased to 99% after 15 h of reaction. The XRD of this solid product showed peaks only due to ZnO, which indicated almost complete conversion of the hydroxide precursor to ZnO (Figure 2c). The increase in pH also made the conversion faster, as pure ZnO phase was obtained after 2 h of reaction (Table 1). Notably, only at a pH >10.9 was KOH without polyamine sufficient to form phase-pure ZnO (Table 1 and Figure S5 in the Supporting Information). The SEM and TEM images of the ZnO formed with PAH (15 kDa) at pH 8.6 show interesting differences in the sizes and morphologies compared with those obtained under neutral conditions (Figure 2a,b and Figure S4 in the Supporting Information). Instead of spindle-like shapes, at pH 8.6 the 2 mg mL^{-1} PAH solution yielded entirely rod-shaped ZnO particles. The rod-shaped particles are of width 300–500 nm and length 800–1700 nm. Comparison of the shapes reveals that the morphological changes are prominent along the longitudinal direction. At higher pH, more of the ZnO nanoparticles are probably accumulating on the pointed ends of the spindles, thereby converting them into a rounded-end rod-shaped morphology. So, the polyamines not only help in the mineralization of ZnO, but also control the shapes of the particles. Together, the presence of polyamine and the pH of the solution are critical in the mineralization process.

The presence of polyamines in the thoroughly washed and dried ZnO particles was monitored by FTIR and confocal micro-Raman analyses. The confocal micro-Raman spectra of the as-synthesized ZnO and PAH are shown in Figure 3a and b and Figure S6 in the Supporting Information. The Raman shift at 441 cm^{-1} is the nonpolar optical phonon E_{2H} mode, which corresponds to the band characteristic of the wurtzite phase. The appearance of the longitudinal optical

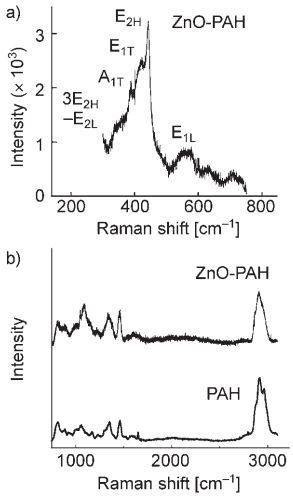

Figure 3. Confocal micro-Raman spectra of ZnO prepared from the precursor and PAH (15 kDa, 2.0 mg mL^{-1}) at RT and pH 8.6 in the spectral ranges a) 150–800 and b) 750–3100 cm^{-1}; b) also shows the spectrum from PAH for comparison.

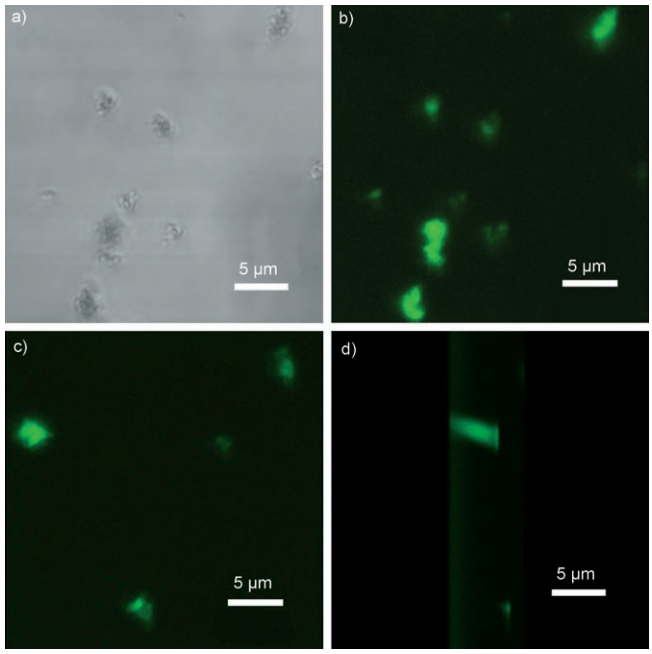

Figure 4. a) Bright-field and b) confocal images of ZnO spindles prepared with PLL-FITC (150 kDa, 2 mg mL^{-1}) at RT and pH 7.5. c),d) Confocal images showing top and side views, respectively.

(E_{1L}) mode at 567 cm^{-1} is attributed to the formation of an oxygen vacancy, or other defect states. Other Raman shifts at 339 and 388 cm^{-1} can be assigned to $3E_{2H}$–E_{2L} and A_{1T} modes, respectively.[15] The distinct band around 2923 cm^{-1} in both the FTIR (see Figure S7 in the Supporting Information) and Raman spectra corresponds to the C–H stretching frequency of the methylene groups of PAH. From the IR and Raman spectra it is clear that polyamines are incorporated or trapped inside the structure during ZnO formation. Even after several washings and centrifugation, the polyamines remained attached to the particles. Thermogravimetric analysis (TGA) of the as-synthesized sample showed a weight loss in the temperature range 200–600 °C, which corresponds to the decomposition of the polyamine. The calculated polyamine content was 16 wt. % of the sample. This result indicates that the polyamines become attached to the particles while catalysing the mineralization of ZnO.

To further locate the presence of polyamines in the ZnO structure, fluorescein isothiocyanate (FITC)-tagged PLL was used to prepare ZnO and confocal microscopic analysis was carried out. From the confocal and bright-field images in Figure 4, it is clear that the PLL-FITC molecules are trapped inside the ZnO matrix. The confocal image of the particles appears as a bright green circle in the top view and as elongated particles in the side view. The presence of polyamine suggests that it may impart functionality to the ZnO nanoparticles that directs the self-assembly process and leads to the observed morphological changes.

Mechanism: Recently, there has been much effort in trying to understand the function of proteins and other biomolecules in biomineralization.[1,2,16] Many in vitro studies have demonstrated the importance of proteins and peptides in controlling the nucleation and/or growth of crystals.[17] Biominerals are usually formed at the surface of organic matrices.[18] These interactions between inorganic species and organic matrices affect not only the particle size and habit of nucleating crystals, but also the stability of intermediate phases by dropping the activation energy required for the formation of specific crystal faces.[19] The organic templates nucleate the mineral by controlling its crystallographic orientation and growth, by imitating the lattice of a two-dimensional face, or by the stereochemistry of the functional groups at the interface.[20] Recent studies suggest that an epitaxial or geometrical match between macromolecules and crystalline faces is not essential. Instead, the charge density on the crystalline faces, and thus the electrostatic attraction, is alone sufficient for heterogeneous nucleation.[21] Further, the surface-stabilized nanoparticles, as nanoscale building blocks, can spontaneously assemble into various morphologically controlled or highly ordered nanostructures.[22] We propose here a similar mechanism of formation and assembly of ZnO nanoparticles. The formation mechanism is shown schematically in Figure 5. The initially precipitated precursor particles have a flake-like morphology; after addition of polyamines at different pH values, the particles undergo morphological changes to produce ZnO nanostructures.

At the pH of ≈7.3 used in our experiments, the amine groups of the polyamine ($pK_a \approx 9$–11) are positively charged. Therefore, the nucleation mechanism may involve an electrostatic attraction between the positively charged NH_3^+ groups of polyamine and the surface oxygen atoms of Zn-OH groups. Under the reactions conditions employed, the polyamine chains are dispersed mainly as random coils, which when adsorbed on to a surface can undergo coil-to-

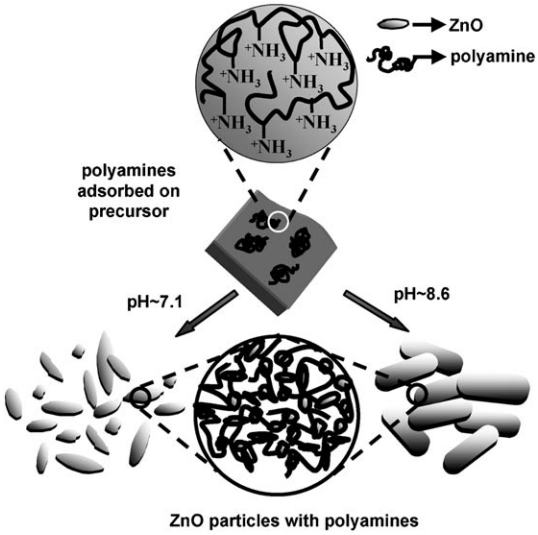

Figure 5. Schematic illustration of the ZnO morphological changes occurring on addition of the polyamine and zinc hydroxide precursor under different reaction conditions. The enlarged view (top) represents the polyamine chains adsorbed on the precursor surface and (bottom) the assembly of nanoparticles by the polyamine chains.

globule transitions.[23] Such adsorption of polyamines leads to accumulation of many NH_3^+ groups at a confined space on the inorganic surface (Figure 5). This may initiate the dehydration of hydroxides to form ZnO, similar to the case of polyamine-induced silica condensation in biosilicification processes taking place under ambient pH conditions. But at pH ≈ 7, in addition to ammonium groups there are about 10% of deprotonated basic amine groups in PAH, which can also catalyse the hydroxide condensation. Amine-based small molecules are known to mineralize ZnO, though generally under alkaline conditions.[7d,8b] To find out the role of ammonium groups, PDADMAC was used as the polycation, which has permanent tertiary ammonium groups. Under similar conditions, the PDADMAC could also mineralize ZnO from the hydroxide precursors (Table 1 and Figure S8 in the Supporting Information). Hence, it is inferred that in our case the ammonium groups of the polyamine are mainly responsible for the mineralization process.

The importance of electrostatic interaction between the precursor and polyamine was verified at an increased ionic strength of the solution by adding KNO_3 to suppress the interaction by forming an electrical double layer. In the presence of 0.2 M KNO_3, the polyamines did not yield any ZnO from the hydroxide precursor at neutral and higher pH values (7.0–11.0). This finding suggests that electrostatic interaction is essential for ZnO mineralization. In addition, it also explains the fact that the use of $Zn(NO_3)_2$ instead of $Zn(OH)_2$ as precursor was not successful in preparing ZnO. The ZnO (wurtzite) structure has several polar faces, which can bind with charged species on their surface. The polar basal face (0001), often called the zinc-terminated face, is composed of zinc atoms, whereas the $(000\bar{1})$ face, referred to as the oxygen-terminated face, is occupied by oxygen atoms. So, the polyamines are expected to preferentially interact with the $(000\bar{1})$ face, which may also be the cause of the amine-containing peptides exhibiting stronger binding for ZnO.[11b]

The surface-specific interaction of PAH molecules with ZnO would lead to a directional orientation of the assembled structure, in which the formed ZnO nanoparticles will have a tendency to assemble onto the PAH molecules preferentially sitting on ZnO $(000\bar{1})$ planes. This would generate a one-dimensional anisotropic growth along the $[000\bar{1}]$ direction resulting in spindles and rods. Consequently, the polyamine molecules would become entrapped in the ZnO structure, thus resulting in a porous structure. To confirm this proposal, high-resolution TEM (HRTEM) analysis was carried out. The HRTEM images in Figure 6 show that the

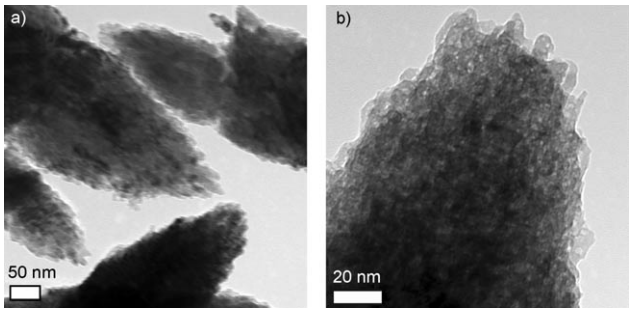

Figure 6. a,b) HRTEM images with different magnifications of ZnO spindles prepared with PAH (15 kDa, 0.8 mg mL^{-1}) at RT, pH 7.4 and a reaction duration of 15 h.

ZnO spindles are aggregates of many nanosized particles and have a porous structure. The assembled particulates are of sizes 10–20 nm, which are comparable with the crystallite size of ZnO estimated from XRD. The porosity of the ZnO particles calcined at 550 °C was evaluated by N_2 physisorption studies. It revealed a specific surface area of 53.0 m^2 g^{-1} and a total pore volume of 0.3954 cm^3 g^{-1} with pore sizes of 2–30 nm (see Figure S9 in the Supporting Information).

Optical properties: The optical properties of the as-synthesized ZnO particles were studied. The band gap of the ZnO powder was evaluated by ultraviolet diffuse reflectance spectroscopy (UV-DRS; Figure 7 a,b). The excitonic absorption peak centred at 379 nm corresponds to a band gap of 3.27 eV. The photoluminescence (PL) spectra of ZnO were measured with an excitation wavelength of 325 nm at room temperature to examine the quality of the product. Figure 7 c and d show the PL spectra for the samples prepared with PAH with molecular weights of 70 and 15 KDa at pH 7.3 and 8.6, respectively, and commercially available ZnO. All the samples exhibit a strong UV emission peak at 384 nm, which corresponds to the near-band-edge emission of ZnO due to annihilation of excitons. In contrast to the commercial sample, the synthesized ZnO samples showed a relatively broad green-light emission at ≈538 nm. Although this emission has been reported many times, the nature of

the defect is still a matter of discussion, the oxygen vacancies being the most likely candidate.[24] The green emission is a result of the radiative recombination of a photogenerated hole with an electron occupying these oxygen vacancies. This peak is comparatively more intense in the case of the sample prepared at neutral pH. It was reported that oxygen vacancies responsible for green emission are located at surfaces, and a higher surface area-to-volume ratio together with a rougher surface favour surface oxygen vacancies.[24b] Moreover, the full-width-at-half-maximum of the UV emission in the PL spectrum is related to crystal quality, and the broadening of the PL line width relative to that of bulk ZnO is sometimes attributed to homogeneously distributed surface impurities or the presence of dopants, which in our case may be due to the presence of polyamines or surface defects.[25] Thus, it is inferred that the polyamine-mediated ZnO mineralization can alter the electronic structure of the nanoparticle surface, and thus can regulate the surface morphology as well as the optical quality of ZnO nanostructures under different synthesis conditions.

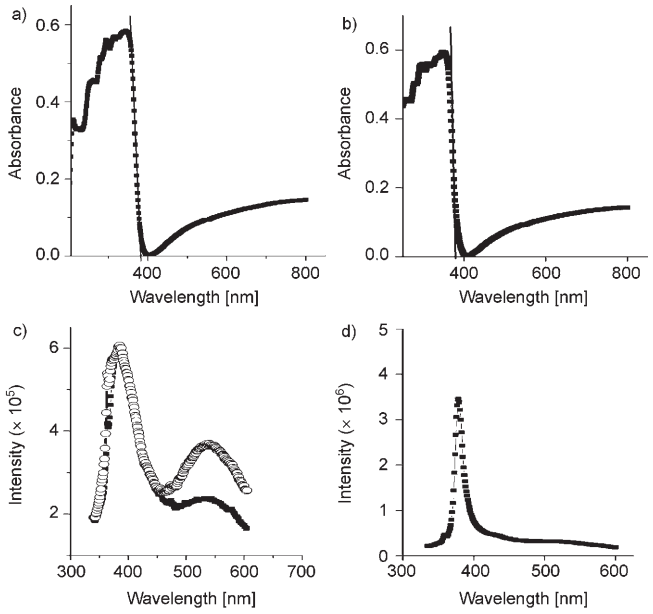

Figure 7. UV/Vis absorption spectra for ZnO prepared from the precursor and a) PAH (70 kDa) at pH 7.3 or b) PAH (15 kDa) at pH 8.6. The tangent used for band-gap calculation is also shown. c) PL spectra of the ZnO obtained with PAH (70 kDa, ○) and PAH (15 kDa, ■) at pH 7.3 and 8.6, respectively. d) PL spectrum of the ZnO available commercially from Sigma–Aldrich.

Conclusion

We have demonstrated a versatile method of synthesizing ZnO nanoparticles that subsequently assemble into spindle- or rod-shaped structures. These observed morphological transformations open up the possibility of controlling the shape and size of the assembled particles by changing the types of polyamines and polypeptides or their conformations. Importantly, the "green" conditions (RT and neutral pH) employed for synthesizing ZnO spindles may lead to potential application of the method. In particular, the technique will be useful for patterning and synthesizing ZnO in or on a substrate without causing any damage to the substrate or species already present on the substrate (see Figure S10 in the Supporting Information). The prominent green emission, which is a signature of oxygen deficiency and the intensity of which can be controlled, may result in a better sensor and catalytic activity.

Experimental Section

Materials: Zinc nitrate hexahydrate ($Zn(NO_3)_2{\cdot}6H_2O$) and potassium hydroxide (KOH) were obtained from SD Fine Chemicals, India. PAH (15 and 70 kDa), PLL (150 and 1–5 kDa), FITC-tagged PLL (30–70 kDa), PDADMAC (100–200 kDa) and ZnO were procured from Sigma–Aldrich and used as received. All the solutions were prepared with deionized water.

Synthesis: Freshly prepared zinc hydroxide was used as the precursor in the synthesis of ZnO. The precursor was prepared by mixing equal volumes of 0.1 M $Zn(NO_3)_2{\cdot}6H_2O$ and 0.2 M KOH in an ice bath (≈4 °C). The produced white precipitate was immediately centrifuged and washed four or five times with distilled water. XRD of the white precipitate showed peaks due to $Zn(OH)_2$ (JCPDS: 20–1435; Figure 1b). AAS analysis of the supernatant showed a 95% conversion of $Zn(NO_3)_2$ to the hydroxide precursor. The washed precipitate was re-dispersed in distilled water to give a zinc hydroxide precursor concentration of 0.1 M for further use (pH 7.6). In a typical synthesis of ZnO, the as-prepared precursor (5 mL) was mixed with PAH (70 kDa) solution. The final concentration of PAH was 2 mg mL^{-1} and the pH was 7.3. The solution was stirred at room temperature (25–27 °C) for various times ranging from 2 to 15 h. The pH of the solution slightly decreased to 7.1 after the reaction. The obtained products were collected by centrifugation followed by washing with distilled water and acetone and then drying at room temperature. Other polyamines and polypeptides were similarly used under various conditions as described in Table 1. Wherever needed, the reaction was carried out under varied pH conditions by adding the required amount (5–400 μL) of 0.2 M KOH solution.

Characterization: Powder XRD patterns were recorded on a Siemens (Cheshire, UK) D5000 X-ray diffractometer by means of CuKα (λ = 1.5406 Å) radiation at 40 kV and 30 mA with a standard monochromator equipped with a Ni filter. The powder XRD patterns were used to identify the crystalline phases of the precipitated powder and to estimate the crystallite size using the Debye–Scherrer formula [$L(hkl) = 0.9\lambda/\Delta(hkl)\cos\theta$], where λ is the X-ray wavelength, θ is the Bragg angle and Δ is the full width of the diffraction line (hkl) at half maximum intensity. A transmission electron microscope (Philips Technai G2 FE1 F12, operating at 80–100 kV) was used to investigate the morphology and size of the particles. The samples for TEM were prepared by dispersing the material in ethanol by ultrasonication and drop-drying onto a formvar-coated copper grid. HRTEM was carried out on a JEOL TEM 2010 microscope operating at 200 kV. SEM analyses were performed by using a Hitachi S-3000N scanning electron microscope operated at 10 kV. Optical imaging was carried out in a confocal microscope (Zeiss LSM Meta) and the data were analysed with a laser scanning microscope (LSM) image examiner. FTIR spectra were recorded at 4000–400 cm^{-1} on a Nicolet Nexus 670 spectrometer equipped with a DTGS KBr detector.

Confocal micro-Raman spectra were recorded by using a Horiba Jobin-Yvon LabRam HR spectrometer with a 17 mW internal He–Ne laser source of excitation wavelength 632.8 nm. UV-DRS analysis was carried out on a GBC UV/Vis Cintra 10/20/40 spectrometer with KBr-diluted pellets of solid samples and pure KBr as the reference. The room-temperature PL spectra were obtained by means of a Jobin-Yvon Fluorolog-3

spectrofluorometer and the 325 nm excitation line of a xenon lamp (450 W). The samples for PL studies were prepared by dispersing small amounts of ZnO powder in ethanol by ultrasonication. All of these samples were maintained at the same concentration. Elemental analysis was carried out by AAS with a Perkin–Elmer AAnalyst 300 spectrometer and TGA was performed with a Mettler Toledo STARe TG analyser in a N_2 atmosphere, with a heating rate of 10 °C min^{-1} from 25 to 1000 °C. N_2 physisorption measurements were recorded with a Quantachrome Autosorb automated gas sorption system. The sample was calcined at 550 °C for 4 h at the rate of 2 °C min^{-1} prior to surface area analysis.

Acknowledgement

R.K.R. thanks the DST, India, and IICT, India, for sponsoring this research through the DST fast-track scheme. G.B. thanks the UGC, India, for a JRF fellowship.

[1] N. Kröger, R. Deutzmann, M. Sumper, *Science* **1999**, *286*, 1129–1132.
[2] K. Shimizu, J. Cha, G. D. Stucky, D. E. Morse, *Proc. Natl. Acad. Sci. USA* **1998**, *95*, 6234–6238.
[3] a) H. R. Luckarift, M. B. Dickerson, K. H. Sandhage, J. C. Spain, *Small* **2006**, *2*, 640–643; b) R. K. Rana, V. S. Murthy, J. Yu, M. S. Wong, *Adv. Mater.* **2005**, *17*, 1145–1150; c) R. Muñoz-Espí, Y. Qi, I. Lieberwirth, C. M. Gómez, G. Wegner, *Chem. Eur. J.* **2006**, *12*, 118–129; d) A. Bharde, D. Rautaray, V. Bansal, A. Ahmad, I. Sarkar, S. M. Yusuf, M. Sastry, *Small* **2006**, *2*, 135–141; e) D. D. Archibald, S. Mann, *Nature* **1993**, *364*, 430–433; f) H. Yang, N. Coombs, G. A. Ozin, *Nature* **1997**, *386*, 692–695; g) K. Ichikawa, N. Shimomura, M. Yamada, N. Ohkubo, *Chem. Eur. J.* **2003**, *9*, 3235–3241.
[4] a) X. Wang, C. J. Summers, Z. L. Wang, *Nano Lett.* **2004**, *4*, 423–426; b) K. Maeda, T. Takata, M. Hara, N. Saito, Y. Inoue, H. Kobayashi, K. Domen, *J. Am. Chem. Soc.* **2005**, *127*, 8286–8287.
[5] M. H. Huang, S. Mao, H. Feick, H. Yan, Y. Wu, H. Kind, E. Weber, R. Russo, P. Yang, *Science* **2001**, *292*, 1897–1899.
[6] Y. Xia, P. Yang, Y. Sun, Y. Wu, B. Mayers, B. Gates, Y. Yin, F. Kim, H. Yan, *Adv. Mater.* **2003**, *15*, 353–389.
[7] a) H. Yan, R. He, J. Johnson, M. Law, R. J. Saykally, P. Yang, *J. Am. Chem. Soc.* **2003**, *125*, 4728–4729; b) X. Y. Kong, Y. Ding, R. S. Yang, Z. L. Wang, *Science* **2004**, *303*, 1348–1351; c) L. Vayssieres, K. Keis, A. Hagfeldt, S. E. Lindquist, *Chem. Mater.* **2001**, *13*, 4395–4398; d) B. Liu, H. C. Zeng, *J. Am. Chem. Soc.* **2003**, *125*, 4430–4431; e) N. Uekawa, R. Yamashita, Y. J. Wu, K. Kakegawa, *Phys. Chem. Chem. Phys.* **2004**, *6*, 442–446; f) W. Peng, S. Qu, G. Cong, Z. Wang, *Cryst. Growth Des.* **2006**, *6*, 1518–1522; g) B. Cheng, E. T. Samulski, *Chem. Commun.* **2004**, 986–987; h) Y. Ishikawa, Y. Shimizu, T. Sasaki, N. Koshizaki, *J. Colloid Interface Sci.* **2006**, *300*, 612–615; i) Y. Liu, Y. Chu, L.-L. Li, L. H. Dong, Y.-J. Zhuo, *Chem. Eur. J.* **2007**, *13*, 6667–6673.
[8] a) H. L. Cao, X. F. Qian, Q. Gong, W. M. Du, X. D. Ma, Z. K. Zhu, *Nanotechnology* **2006**, *17*, 3632–3636; b) B. Liu, H. C. Zeng, *Langmuir* **2004**, *20*, 4196–4204.
[9] A. P. A. Oliveira, J. F. Hochepied, F. Grillon, M. H. Berger, *Chem. Mater.* **2003**, *15*, 3202–3207.
[10] a) D. Kisailus, B. Schwenzer, J. Gomm, J. C. Weaver, D. E. Morse, *J. Am. Chem. Soc.* **2006**, *128*, 10276–10280; b) Z. Zhang, H. Yu, X. Shao, M. Han, *Chem. Eur. J.* **2005**, 11, 3149–3154.
[11] a) L. P. Bauermann, A. del Campo, J. Bill, F. Aldinger, *Chem. Mater.* **2006**, *18*, 2016–2020; b) M. Umetsu, M. Mizuta, K. Tsumoto, S. Ohara, S. Takami, H. Watanabe, I. Kumagai, T. Adschiri, *Adv. Mater.* **2005**, *17*, 2571–2575; c) P. Gerstel, R. C. Hoffmann, P. Lipowsky, L. P. H. Jeurgens, J. Bill, F. Aldinger, *Chem. Mater.* **2006**, *18*, 179.
[12] a) K. Gorna, R. Muñoz-Espí, F. Grohn, G. Wegner, *Macromol. Biosci.* **2007**, *7*, 163–173; b) R. V. Kumar, R. Elgamiel, Yu. Koltypin, J. Norwig, A. Gedanken, *J. Cryst. Growth* **2003**, *250*, 409–417; c) A. Taubert, D. Palms, O. Weiss, M. T. Piccini, D. N. Batchelder, *Chem. Mater.* **2002**, *14*, 2594–2601; d) Y. Lin, J. Xie, H. Wang, Y. Li, C. Chavez, S. Y. Lee, S. R. Foltyn, S. A. Crooker, A. K. Burrell, T. M. McCleskey, Q. X. Jia, *Thin Solid Films* **2005**, *492*, 101–104; e) C. Wang, E. Shen, E. Wang, L. Gao, Z. Kang, C. Tian, Y. Lan, C. Zhang, *Mater. Lett.* **2005**, *59*, 2867–2878; f) M. Mo, J. C. Yu, L. Zhang, S.-K. A. Li, *Adv. Mater.* **2005**, *17*, 756–760.
[13] F. Li, Y. Ding, P. Gao, X. Xin, Z. L. Wang, *Angew. Chem.* **2004**, *116*, 5350–5354; *Angew. Chem. Int. Ed.* **2004**, *43*, 5238–5242.
[14] D. S. Golovko, R. Muñoz-Espí, G. Wegner, *Langmuir* **2007**, *23*, 3566–3569.
[15] a) T. C. Damen, S. P. S. Porto, B. Tell, *Phys. Rev.* **1966**, *142*, 570–574; b) S. Chen, Y. Liu, C. Shao, R. Mu, Y. Lu, J. Zhang, D. Shen, X. Fan, *Adv. Mater.* **2005**, *17*, 586–590; c) J. Liu, X. Huang, K. M. Sulieman, F. Sun, X. He, *J. Phys. Chem. B* **2006**, *110*, 10612–10618.
[16] L. Silverman, A. L. Boskey, *Calcif. Tissue Int.* **2004**, *75*, 494–501.
[17] a) S. Busch, U. Schwarz, R. Kniep, *Adv. Funct. Mater.* **2003**, *13*, 189–198; b) O. Grassmann, G. Müller, P. Lobmann, *Chem. Mater.* **2002**, *14*, 4530–4535; c) A. Bigi, S. Panzavolta, N. Roveri, *Biomaterials* **1998**, *19*, 739–744.
[18] a) E. Dujardin, S. Mann, *Adv. Mater.* **2002**, *14*, 775–788; b) H. H. Teng, P. M. Dove, J. J. DeYoreo, *Geochim. Cosmochim. Acta* **1999**, *63*, 2507–2512.
[19] H. Cölfen, S. Mann, *Angew. Chem.* **2003**, *115*, 2452–2468; *Angew. Chem. Int. Ed.* **2003**, *42*, 2350–2365.
[20] G. Falini, *Int. J. Inorg. Mater.* **2000**, *2*, 455–461.
[21] a) D. Volkmer, M. Fricke, M. Gleiche, L. Chi, *Mater. Sci. Eng. C* **2005**, *25*, 161–167; b) T. Coradin, S. Bah, J. Livage, *Colloids Surf. B* **2004**, *35*, 53–58.
[22] a) A. S. Deshpande, I. Burgert, O. Paris, *Small* **2006**, *2*, 994–998; b) J. Yu, V. S. Murthy, R. K. Rana, M. S. Wong, *Chem. Commun.* **2006**, 1097; c) M. S. Toprak, B. J. Mckenna, M. Mikhaylova, J. H. Waite, G. D. Stucky, *Adv. Mater.* **2007**, *19*, 1362.
[23] a) L. J. Kirwan, G. Papastavrou, M. Borkovec, S. H. Behrens, *Nano Lett.* **2004**, *4*, 149–152; b) S. Minko, A. Kiriy, G. Gorodyska, M. Stamm, *J. Am. Chem. Soc.* **2002**, *124*, 3218–3219.
[24] a) F. Q. He, Y. P. Zhao, *Appl. Phys. Lett.* **2006**, *88*, 193113; b) M. H. Huang, Y. Wu, H. Feick, N. Tran, E. Weber, P. Yang, *Adv. Mater.* **2001**, *13*, 113–116.
[25] B. Kumar, H. Gong, S. Y. Chow, S. Tripathy, Y. Hua, *Appl. Phys. Lett.* **2006**, *89*, 071922–071923.

Received: January 22, 2008
Published online: June 5, 2008

